Check for updates

Synthesis and properties of branched alcohol alkoxylate sulfates

Yang Yue, [ID] [ab] Cao Shengti, [ab] Gao Chunxin, [ab] Huo Yueqing [ab] and Liu Xiaochen*[ab]

In this study, three branched alcohol alkoxylate sulfates ($C_{10}E_3S$, $C_{10}E_3P_3S$ and $C_{10}P_3E_3S$) were synthesized using a gas SO_3 membrane sulfonation device. Their structures were characterized by FT-IR spectroscopy, ESI-MS, and TGA. In order to investigate the effects of hydrophobic carbon chains, polyoxyethylene groups (EO) and polyoxypropylene groups (PO) on the product properties, the static surface tension, dynamic surface tension, contact angle, foam properties, wetting properties, and emulsification properties were tested. The results showed that $C_{10}P_3E_3S$ exhibited a smaller maximum adsorption (1.31 μmol m^{-2}). In the test of alkali wettability, $C_{10}P_3E_3S$ also exhibited more excellent performance, indicating that it can be used as an alkali penetrant in printing and dyeing pretreatment. Meanwhile, the poor foam performance of $C_{10}E_3P_3S$ suggests that the position of the PO group in the molecule may significantly affect its performance due to steric hindrance. Owing to the above properties, indicating $C_{10}E_3P_3S$ is a low-foaming surfactant.

1 Introduction

Surfactants are a class of organic compounds that have both hydrophilic (polar) groups and hydrophobic (non-polar) groups;[1] these compounds are active on the surface[2] and have high ability and efficiency to reduce surface and interfacial tensions. Additionally, under certain conditions, surfactants can self-assemble to form molecularly ordered assemblies.[3] Owing to these properties, surfactants are widely applied in various fields, including the food industry,[4] pharmaceuticals,[5] dyeing,[6] agriculture[7] and environmental protection.[8]

In comparison with linear surfactants, surfactants featuring branched alkyl chains possess numerous advantages, including good water solubility, excellent wettability, rapid defoaming ability, *etc.*[9] The properties of branched surfactants have attracted the attention of researchers. For example, Yada *et al.*[10] synthesized a series of EO-type nonionic surfactant (AEO$_n$), and it was suggested that multi-branched EO-based nonionic surfactants demonstrate lower surface tensions than single straight-chain EO-based surfactants (less than 30 mN m^{-1}). Moreover, branched ionic surfactants containing EO groups exhibit outstanding properties. For instance, by synthesizing $C_{14}E_nS$ ($n = 1, 2,$ and 4) using the Guerbet reaction, Jin *et al.*[11] found that the introduction of EO groups between the hydrophilic and hydrophobic groups of branched surfactant molecules can reduce CMC (critical micelle concentration), γ_{cmc} (surface tension), and Krafft points. In addition, Zhang *et al.*[12]

synthesized branched-chain alcohol polyoxyethylene ether carboxylates (AECs), which are surfactants with remarkable wetting ability, characterized by strong emulsifying ability, good foaming ability, and potent detergency. Chen *et al.*[13] investigated the relationship between the molecular structure and solution/interfacial properties of branched surfactants (C_nP_mS, $n = 8, 10,$ and 13 and $m = 3, 6,$ and 9). The results indicated that the PPO spacer group in the molecule indeed complements the branched chain, enhancing its relatively poor detergency. Consequently, the product is anticipated to replace sodium lauryl sulfate in cleaning products.

Alcohol ether sulfates are crucial components of surfactants, and researchers have carried out a series of studies on them, exploring the impacts of EO and PO groups on their properties and functions. The EO group is hydrophilic, and as the degree of ethoxylation increases, the surfactant molecule can form stronger hydrogen bonding interactions with water, resulting in increased solubility;[14] this may provide support for further studies on interfacial adsorption behavior. In addition, in the study of coal dust adsorption, Hussain *et al.*[15] found that the EO group of AE_3S could adsorb free Na$^+$ in the surrounding solution, forming a double-layer adsorption structure and thus achieving a high adsorption density. The PO group also affects the interfacial properties of surfactants. Zhang *et al.*[16] found that when the model oil is the same, the lowest equilibrium interfacial tension of $C_{16}P_mS$ ($m = 1, 2,$ and 3) decreases with the increasing number of PO groups. For example, $C_{16}E_3S$ reduces the oil–water interfacial tension to 0.026 mN m^{-1}. Besides, Liu *et al.*[17] found that the interfacial tension between $C_{12}P_nS$ solution and *n*-heptane can reach 0.01 mN m^{-1}.18 When EO and PO groups are both present, the surfactant is called extended surfactant. In

aChina Research Institute of Daily Chemical Industry, Taiyuan 030001, Shanxi, China. E-mail: liuren517@163.com

bShanxi Key Laboratory of Functional Surfactants, Taiyuan 030001, Shanxi, China

addition to reducing interfacial tension to ultra-low levels,[19] these products also have good water solubility, excellent foam properties and biodegradability. Chen et al.[20] synthesized a series of C_{16-18} extended surfactants and then compared them to a series of linear surfactants. The results showed that the water solubility, salt resistance, and gelation properties of these extended surfactants were significantly affected by the embedded nonionic chain structure and hydrocarbon structure. Additionally, Huang et al.[21] found that the introduction of PO groups after EO groups enhances the emulsifying properties of extended surfactants and reduces their foaming ability.

Herein, three branched alcohol ether sulfates, $C_{10}E_3S$, $C_{10}E_3P_3S$ and $C_{10}P_3E_3S$, were successfully synthesized using 2-propylheptanol polyoxyethylene ether, 2-propylheptanol polyoxyethylene polyoxypropylene ether and 2-propylheptanol polyoxypropylene polyoxyethylene ether by a gas SO_3 membrane sulfonation device, and the products were characterized by FT-IR spectroscopy, ESI-MS and TGA. Furthermore, the surface properties and adsorption behaviors of these surfactants were also studied.

The results suggest that the position of PO groups may have an effect on the dynamic surface tension, static surface tension, and contact angle due to steric hindrance, and thus have an impact on the emulsification properties.

2 Experimental section

2.1 Materials

Branched alcohol alkoxylate ether, including 2-propylheptanol polyoxyethylene ether ($C_{10}E_3$), 2-propylheptanol polyoxyethylene polyoxypropylene ether ($C_{10}E_3P_3$), 2-propylheptanol polyoxypropylene polyoxyethylene ether ($C_{10}P_3E_3$), were acquired from Sinolight Chemicals Co., Ltd.

2.2 Synthesis of surfactants

The products were synthesized using an SO_3 gas membrane sulfonation device. The raw material reacted with SO_3 in the sulfonation tube, and the sample was obtained after the reactants flowed out and were neutralized with a 20 wt% NaOH solution. Taking the synthesis of $C_{10}E_3S$ as an example, the reaction process is shown in Fig. 1. Other reaction processes are shown in Fig. S1 and S2.

2.3 Structural characterization

Fourier transform infrared (FT-IR) spectroscopy (VERTEX70, Germany) was used to detect functional groups in the samples. Electrospray mass spectrometry (HPLC-2998-QDa, Waters) was used to determine the relative molecular mass of compounds. Additionally, the solid content, mineral sulfate content, anionic-active matter content and unsulfated matter content of $C_{10}E_3S$, $C_{10}E_3P_3S$ and $C_{10}P_3E_3S$ were tested. The results are shown in Table S1.

2.4 Thermal performance analysis

The thermal performance analysis (TGA, HTG-3, China) was measured using an HTG-3 precision thermobalance. Before testing, the samples were baked in an oven at 105 °C until a constant weight was obtained.

2.5 Static surface tension

The static surface tension of $C_{10}E_3S$, $C_{10}E_3P_3S$, $C_{10}P_3E_3S$ were measured by Wilhelmy plate method at 25 ± 0.1 °C by K12 (KRÜSS, Germany). The solutions of samples were prepared and allowed to stand for 24 hours to ensure the experimental accuracy. During the test, the plate was heated until it glowed red-hot. These steps ensured that the surface tension of water was 72 ± 0.2 mN m^{-1}.

2.6 Dynamic surface tension

The dynamic surface tension of the samples was measured using a dynamic surface tension meter (BP100, KRÜSS, Germany) at 25 °C ± 0.1 °C. Prior to the measurement, the solutions of samples were allowed to stand for 8 hours to achieve equilibrium. When testing, the surface age was 200 s.

2.7 Contact angle measurement

The contact angle measuring instrument (DSA25S, KRÜSS, Germany) was used to measure the contact angle and its morphology of a sample drop applied to a paraffin film at 25 °C ± 0.1 °C. After a liquid droplet landed on the paraffin film, a CCD camera was used to record its morphology for the next two minutes. The concentration of the surfactant solution was 1 g L^{-1}.
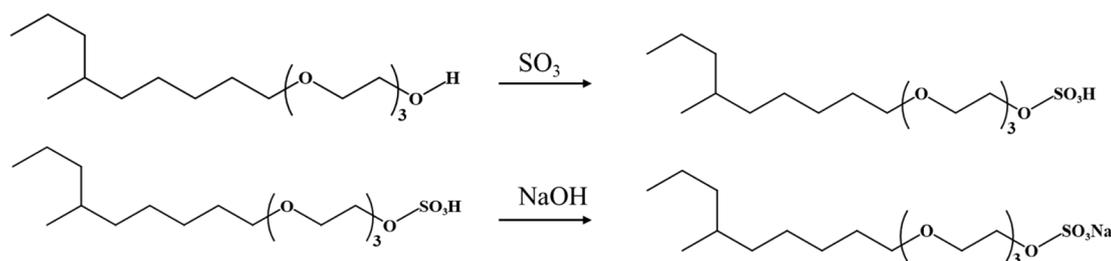

Fig. 1 The reaction process for the synthesis of $C_{10}E_3S$.

2.8 Emulsifying power

Before the experiment, the preparation of a 1 g L^{-1} surfactant solution at 25 °C was necessary. Then, 40 mL of the surfactant solution was added into a stoppered test tube, followed by addition of another 40 mL of paraffin liquid, and the mixture was shaken 5 times after stoppering and then allowed to stand for 1 min. Then, the above operation was repeated 5 times, and during the last shaking, timing was started and the time required for the lower layer to separate out 10 mL of water was recorded. The test was repeated for three times, and the average value and standard deviation of the phase separation time were calculated.

2.9 Wettability

A series of 1 g per L surfactant solutions was prepared at 25 °C, and the wettability of the surfactant under different alkali concentrations was determined by the canvas sheet settling method. The canvas sheets were immersed in the surfactant solution using a special experimental folder, and the time for the canvas sheets to fall from the folder was recorded. The final result was the average of five measurements as well as the standard deviation.

2.10 Alkali tolerance

At 25 °C, 1 g per L surfactant solution was prepared, to which different volumes of NaOH solution were added and shaken well to obtain surfactant solutions with different alkali concentrations. The solutions were placed in an oven at 30 °C for 24 h and then observed for turbidity and tested for light transmittance.

2.11 Foam ability and foam stability

The foam ability was determined using modified Ross–Miles method in 25 °C and 50 °C. The foam volume of the system was recorded at 30 s, 60 s, 120 s, 180 s and 300 s. The ratio of the foam volume at 300 s to the foam volume at 30 s was considered as the foam stability. This procedure was repeated for three times, and the average value and standard deviation were calculated.

3 Results and discussion

3.1 Structural characterization

FT-IR spectroscopy is commonly used to characterize the functional groups contained in a substance. As shown in Fig. 2a, the broad band at 3475 cm^{-1} is well known for the stretching vibration modes[22] of OH^-. Additionally, the wide bands between 2920 cm^{-1} and 2850 cm^{-1} are attributed to C–H asymmetric and symmetric stretching vibration bands.[23] The wavenumber near 1110 cm^{-1} is attributed to C–O–C ester bond absorption band.[24] Symmetric stretching vibration band of CH_3^-[25] exhibits at 1465 cm^{-1}. Furthermore, the bands at 1035 cm^{-1} and 1220 cm^{-1} are assigned to symmetric and asymmetric stretching of S=O group, indicating the presence of a sulfate radical. Similarly, the absorption band at 820 cm^{-1} suggests the presence of C–O–S,[16] showing that the samples were successfully sulfonated. In addition, the rocking vibrations at 760 cm^{-1} indicate the presence of $(CH_2)_n^-$ unit,[26] which is attributed to the EO groups. The functional groups showed that the molecular structures of the three substances were similar, indicating that $C_{10}E_3S$, $C_{10}E_3P_3S$, $C_{10}P_3E_3S$, were succesfully synthesized.

ESI-MS can be used to analyze the molecular weight distribution of samples, based on the fact that alcohol ether sulfates can be ionized into negative ions in water. The mass spectra of samples are shown in Fig. 2c.

In the alcohol ether sulfate system, the products are mixtures of sulfates with different EO groups, so their EO addition numbers are statistically significant. In Fig. 2c, the molecular weight of $C_{10}E_mP_nS$ is $260 + 44m + 58n$, and the molecular weight after dissociation and ionization by Na^+ is $237 + 44m + 58n$, where m represents the EO number and n represents the PO number. Taking $C_{10}E_3S$ as an example, $m/z = 281, 325, 369, 413, 457, 501, 545, 589, 633, 677$ represent EO = 1, 2, 3, 4, 5, 6, 7, 8, 9, 10, respectively, which indicates that $C_{10}E_3S$ is a mixture of sulfate salts composed of EO = 1–10. This indicates the presence of sulfate radical, suggesting that sulfonation was successfully achieved. Further analysis and mass spectra of $C_{10}E_3P_3S$ and $C_{10}P_3E_3S$ are shown in Fig. S3.

3.2 Thermal performance analysis

In our study, the thermal decomposition is shown in Fig. 2b. The weight loss process of surfactants can be roughly divided
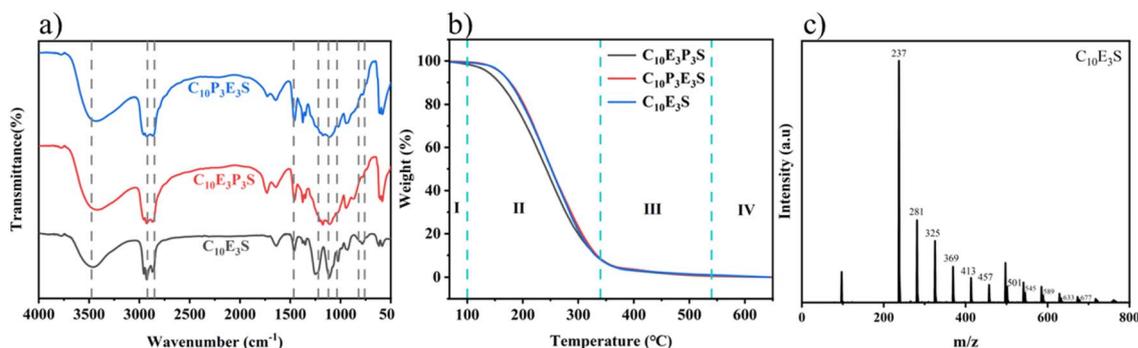
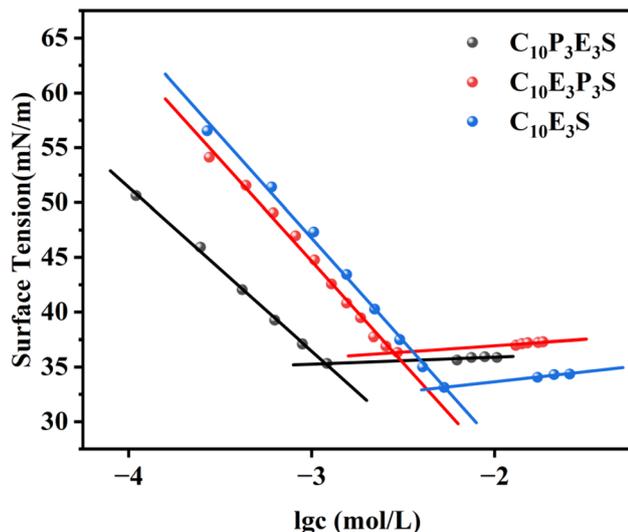Fig. 2 (a) FT-IR spectra, (b) TGA results, and (c) ESI-MS results.

Fig. 3 Static surface tension *versus* the logarithm of the concentration of sample solutions.

into four stages. In the first stage, there is a slight weight loss of the sample which may have occurred due to the presence of minor impurities in the product. In the second stage, the heated decomposition of propoxy and ethoxy may be the reason for the significant weight loss phenomenon in the samples at 140–340 °C. From this figure, the initial decomposition temperatures of the surfactants are as follows: $C_{10}E_3P_3S$ > $C_{10}P_3E_3S$ > $C_{10}E_3S$. This may be attributed to the introduction of heat-intolerant PO groups, which lead to earlier thermal decomposition of PO-containing surfactants. The third stage (340–540 °C) and the fourth stage (>540 °C) indicate that the surfactant was basically decomposed by heating when the decomposition of EO and PO groups was complete.

3.3 Static surface tension

The relationship between the logarithm of the sample concentration and static surface tension is shown in Fig. 3. As the concentration increases, molecules aggregate at the gas–liquid interface and thus decrease the surface tension. When the maximum adsorption amount is reached, the surface tension

tends to a constant value, and under this condition, the lowest point of the curve is usually the critical micelle concentration (CMC) of the surfactant, and the corresponding vertical coordinate is γ_{cmc}. When the concentration continues to rise above the critical micelle concentration, the surfactant molecules aggregate at the gas–liquid interface returns to the interior of the solution, resulting in a slight increase in the surface tension curve. Herein, we also compared one of the commercially available surfactant (AE₃S) with $C_{10}E_3S$, $C_{10}E_3P_3S$ and $C_{10}P_3E_3S$. The results are shown in Table S2, Fig. S4, Tables S3 and S4.

In order to investigate the behavior of the samples at the gas–liquid interface, additional parameters are listed in Table 1. The Gibbs adsorption equation gives Γ_{max} (maximum adsorption)[27] and the average molecular cross-sectional area (A_{min})[28] of the surfactant molecules (eqn (1) and (2)):

$$\Gamma_{max} = -\left(\frac{1}{2.303nRT}\right)\left(\frac{d\gamma}{d \lg c}\right) \quad (1)$$

$$A_{min} = \frac{1}{\Gamma_{max}N_A} \quad (2)$$

where R and T represent the molar gas constant (8.314 J mol⁻¹ K⁻¹) and absolute temperature (298.15 K), respectively. (dγ/d lg c) is the slope of the surface tension γ *versus* lg c below the CMC. For alcohol ether sulfate surfactants, n is usually taken as 2. N_A is Avogadro's constant (6.022 × 10²³). In addition, the micellization Gibbs energy (ΔG_{mic}) and the adsorption Gibbs energy (ΔG_{ads}) can be obtained by calculations using eqn (3) and (4).[29]

$$\Delta G_{mic} = RT \ln\left(\frac{CMC}{55.5}\right) \quad (3)$$

$$\Delta G_{ads} = RT \ln\left(\frac{C_\Pi}{55.5}\right) - 6.022\Pi A \quad (4)$$

where Π is the surface pressure $(\gamma_0 - \gamma_{cmc})$ in the saturated region of surface adsorption, and C_Π is the concentration of the surfactant under surface pressure. The results of the calculations are presented in Table 2.

The negative logarithm pC_{20} of the surfactant concentration required to reduce the surface tension of water by 20 mN m⁻¹ is defined as the surfactant efficiency[30] (eqn (5)):

Table 1 The dynamic surface tension parameters

Sample	c (g L⁻¹)	n	t^* (s)	lg t^*	t_i (s)	t_m (s)	$R_{1/2}$ (mM m⁻¹ s⁻¹)
$C_{10}E_3P_3S$	1.0	0.25	8.32×10^{-2}	−1.08	8.32×10^{-6}	831.76	219.05
	1.0×10^{-1}	0.43	29.18	1.47	0.14	6175.86	0.62
	1.0×10^{-2}	0.17	1.97×10^5	5.29	0.26	1.50×10^{11}	9.76×10^{-5}
	1.0×10^{-3}	0.10	7.94×10^{10}	10.90	7.94	7.94×10^{20}	2.42×10^{-10}
$C_{10}P_3E_3S$	1.0	0.35	5.18×10^{-2}	−1.29	7.20×10^{-5}	37.28	362.10
	1.0×10^{-1}	0.46	18.21	1.26	0.12	2717.80	1.03
	1.0×10^{-2}	0.18	1.09×10^5	5.04	0.36	3.25×10^{10}	1.82×10^{-4}
	1.0×10^{-3}	0.08	1.85×10^{13}	13.27	7.38	4.64×10^{25}	1.07×10^{-12}
$C_{10}E_3S$	1.0	0.24	4.64	0.67	3.16×10^{-4}	6.81×10^4	4.27
	1.0×10^{-1}	0.31	1077.11	3.03	0.64	1.81×10^6	1.84×10^{-2}
	1.0×10^{-2}	0.19	2.34×10^6	6.37	12.74	4.28×10^{11}	8.60×10^{-6}
	1.0×10^{-3}	0.10	2.51×10^{11}	11.40	25.12	2.51×10^{21}	8.29×10^{-11}

Table 2 The static surface tension parameters

Sample	CMC (mmol L^{-1})	γ_{cmc} (mN m^{-1})	Γ_{max} (µmol m^{-2})	A (nm^2)	pC_{20}	ΔG_{mic} (kJ mol^{-1})	ΔG_{ads} (kJ mol^{-1})
C$_{10}$E$_3$P$_3$S	2.87 ± 0.24	36.40 ± 0.04	1.45 ± 0.17	1.03 ± 0.01	3.45 ± 0.01	−24.47 ± 0.20	−24.69 ± 0.21
C$_{10}$P$_3$E$_3$S	1.15 ± 0.15	35.20 ± 0.09	1.30 ± 0.02	1.28 ± 0.01	4.24 ± 0.15	−26.76 ± 0.31	−27.05 ± 0.31
C$_{10}$E$_3$S	5.11 ± 0.10	33.56 ± 0.41	1.64 ± 0.01	1.02 ± 0.01	3.31 ± 0.01	−23.03 ± 0.05	−23.78 ± 0.05

$$pC_{20} = -\lg C_{20} \quad (5)$$

As shown in Table 2, the critical micelle concentration of C$_{10}$E$_3$S was greater than the rest of the samples, and the main driving force for micelle formation was the interaction between hydrophobic groups,[31] which could be attributed to the shorter carbon chain of the surfactant and the smaller van der Waals force between hydrophobic groups, which were not conducive to the formation of micelles, leading to its larger CMC. In addition, the other samples had a lower CMC due to the branching effect and the large steric hindrance between molecules, which made it difficult to form micelles.

Rosen suggested that the standard free energy of transfer of a surfactant molecule from the bulk phase to the interface is related to pC_{20}, and since then, researchers have generally described the parameter that reduces surface tension as pC_{20}.[32] As shown in Table 2, C$_{10}$P$_3$E$_3$S has the highest pC_{20}, indicating that it is the most surface active agent, which is more in line with what is reflected in the rest of the results of this study. In addition, the ΔG_{mic} and ΔG_{ads} of several samples were negative, and the difference between $|\Delta G_{mic}|$ and $|\Delta G_{ads}|$ was not significant, demonstrating that there is no obvious sequence between the formation of molecular micelles of surfactants and their interfacial adsorption behavior.[33]

3.4 Dynamic surface tension

The transfer of surfactant molecules from the bulk phase to the gas–liquid interface is a dynamic process. As the water molecules on the surface are continuously replaced by surfactant molecules, the surface tension decreases continuously. The adsorption of surfactant molecules from the liquid phase to the air–liquid interface is a dynamic process. In order to investigate the surface properties and adsorption modes of the surfactant molecules under non-equilibrium conditions, the dynamic

surface tension curves of the samples at different concentrations were tested separately, as shown in Fig. 4.

Rosen et al. considered the dynamic surface tension curve to be divided into four phases: induction zone, rapid decline zone, meso-equilibrium zone, and equilibrium zone. As can be seen in Fig. 4, when the concentration is low, only the induction zone appears in the curve; at the same time, the induction zone becomes shorter and the time to reach the meso-equilibrium zone is shortened as the concentration increases. In addition, the meso-equilibrium zone is reached faster when the concentration is above the CMC compared to below the CMC, which may be due to the fact that the excess surfactant molecules in the solution of higher concentration have a facilitating effect on their own rapid adsorption to the gas–liquid interface, thus shortening the time required for the surface tension to reach equilibrium.[34] Correspondingly, as can be seen in Fig. 4c, C$_{10}$E$_3$S exhibits a longer induction zone across all concentration ranges and a slower decrease in surface tension in the fast-falling zone than C$_{10}$E$_3$P$_3$S and C$_{10}$P$_3$E$_3$S.

3.4.1 Rosen formula. To analyze the first three regions of the curve even further, Rosen et al.[35] also proposed an empirical equation for surface tension over time:

$$\frac{\gamma_0 - \gamma_t}{\gamma_t - \gamma_{eq}} = \left(\frac{t}{t^*}\right)n \quad (6)$$

To make the expression clearer, taking logarithms of both the left and right sides of the equal sign of eqn (6) yields the following equation:

$$\lg \frac{\gamma_0 - \gamma_t}{\gamma_t - \gamma_{eq}} = n \lg t - n \lg t^* \quad (7)$$

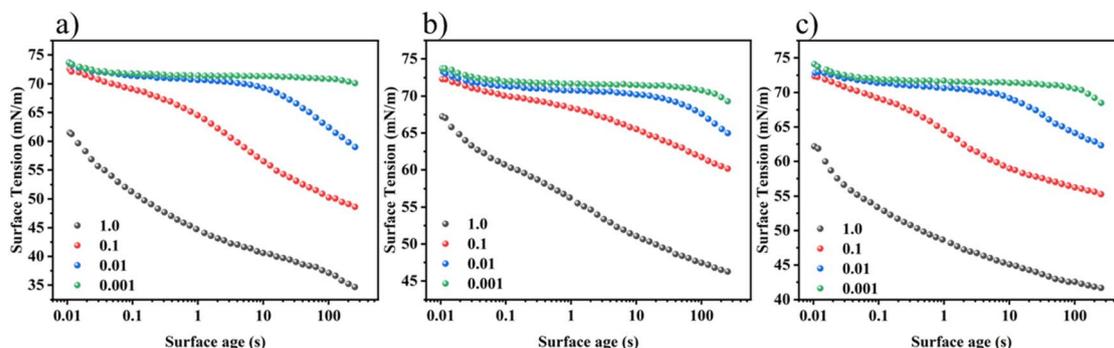In eqn (7) where γ_0 and γ_{eq} are the surface tension and equilibrium surface tension of the pure solvent, respectively; γ_t

Fig. 4 Dynamic surface tension *versus* surface age of the surfactants at different concentrations (g L^{-1}): (a) C$_{10}$P$_3$E$_3$S, (b) C$_{10}$E$_3$S, and (c) C$_{10}$E$_3$P$_3$S.

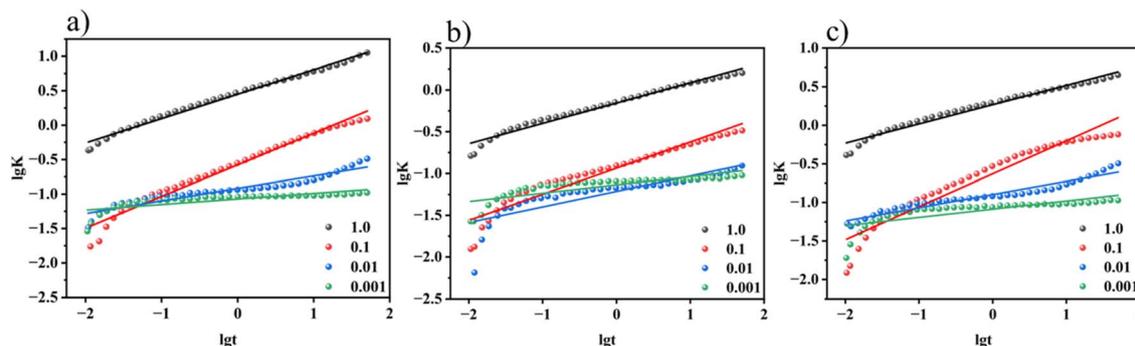**Fig. 5** Analysis of the Rosen model of dynamic surface tension at different concentrations (g L^{-1}) of (a) $C_{10}P_3E_3S$, (b) $C_{10}E_3S$, and (c) $C_{10}E_3P_3S$.

is the surface tension at the moment when the surface age is t, n is a dimensionless constant, and t^* is the time required for γ_t to reach half of $(\gamma_0 - \gamma_{eq})$. K is defined as $(\gamma_0 - \gamma_t)/(\gamma_t - \gamma_{eq})$. The fitted curve obtained by plotting $\lg t$ as the independent variable and $\lg K$ as the dependent variable is shown in Fig. 5.

Meanwhile, t_i is defined as the end time of the induction zone and t_m as the time of the beginning of the meso-equilibrium region, the time parameters t_i and t_m can be obtained by eqn (8) and (9):[36]

$$\lg t_i = \lg t^* - \frac{1}{n} \tag{8}$$

$$\lg t_m = \lg t^* + \frac{1}{n} \tag{9}$$

$R_{1/2}$ is defined as the rate of decrease of surface tension at the moment t^* in the rapidly decreasing region, which can be calculated from eqn (10):[37]

$$R_{1/2} = \frac{\gamma_0 - \gamma_{eq}}{2t^*} \tag{10}$$

The characteristic parameters of dynamic surface tension were calculated, as shown in Table 1.

As shown in Fig. 2, for $C_{10}E_3P_3S$, $C_{10}P_3E_3S$, and $C_{10}E_3S$ surfactants, n increases and then decreases with the increase in concentration, while n reflects the process of surfactant molecules diffusing from the bulk phase to the subsurface layer in the early stage, and the smaller the value of n indicates that its diffusion barrier is lower, which suggests that higher concentrations are favorable for the diffusion of surfactants compared with lower concentrations, which is consistent with the result that surfactants can reach the meso-equilibrium region within a short period of time in the higher concentration region. This is consistent with the result that the surfactant can reach the meso-equilibrium region in a shorter time in the region of higher concentration. This is consistent with the result that the surfactant can reach the equilibrium region in a shorter time in the region of higher concentration, which may be mainly due to the fact that the higher concentration facilitates the diffusion of molecules from the bulk phase to the gas–liquid interface. t^* reflects the adsorption of surfactant molecules from the

subsurface layer to the surface in the later stage, and the larger t^* is, the higher the adsorption barrier is. While t^* is inversely proportional to the concentration, this may be due to the fact that at higher surfactant concentrations, the molecules are more susceptible to electrostatic repulsion, which reduces the diffusion efficiency; another possible reason is that the simultaneous adsorption process increases the surface pressure, which reduces the adsorption vacancies and further improves the resistance to adsorption.

3.4.2 Diffusion-controlled adsorption model. At the beginning of the adsorption process at the gas–liquid interface, monomers adsorb directly from the subsurface, with each molecule occupying an adsorption site after reaching the adsorption interface. As the adsorption process continues, the surface becomes more and more crowded, and there is a reverse adsorption of monomer molecules from the subsurface to the bulk phase. This process can be analyzed using the Ward–Tordai model.[38]

$$\Gamma_t = 2c_0\sqrt{\frac{D_t}{\pi}} - \sqrt{\frac{D}{\pi}}\int_0^t \frac{c_s(t)}{\sqrt{t-\tau}}\mathrm{d}\tau \tag{11}$$

In eqn (11), Γ_t is the surface adsorption at time t, D is the diffusion coefficient, c_0 is the bulk phase concentration, c_s is the subsurface concentration, and τ is a dummy time delay variable. However, the Ward–Tordai equation[39] is so complicated to solve that the short time approximation ($t \to 0$) case and the long time ($t \to \infty$) approximation of the surfactant molecule can be determined by Hansen and Jos' equation:

$$\gamma_{(t)t\to 0} = \gamma_0 - 2nRTc_0\sqrt{\frac{D_t}{\pi}} \tag{12}$$

$$\gamma_{(t)t\to 0} = \gamma_{eq} + \frac{nRT\Gamma^2}{c_0}\sqrt{\frac{\pi}{4D_t}} \tag{13}$$

For eqn (12) and (13), γ_t is the surface tension of the surfactant at time t, γ_0 is the surface tension of pure water, γ_{eq} is the equilibrium surface tension, Γ is the equilibrium surface excess concentration, T is the absolute temperature, R is the gas constant (8.314 J mol^{-1} K^{-1}), and n is usually taken to be 2 for the alcohol ether sulphate surfactants. It can be seen that

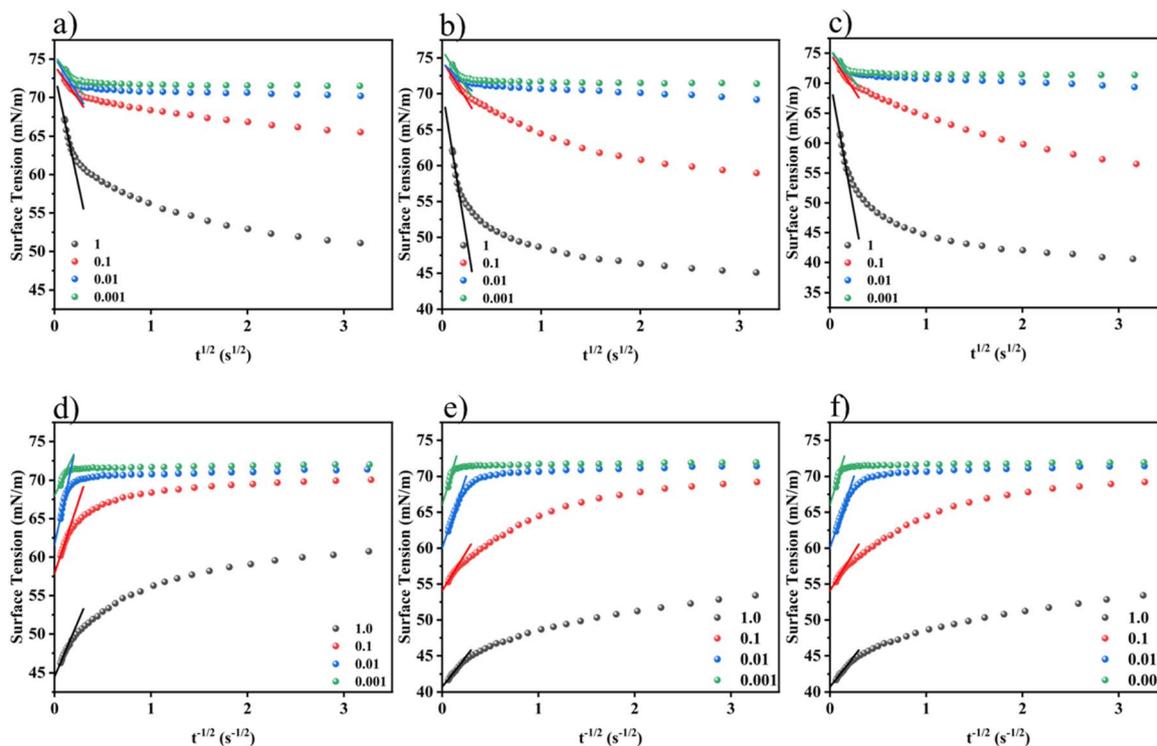**Fig. 6** The diffusion coefficients of the samples calculated at different concentrations (g L^{-1}): (a) and (d) $C_{10}E_3S$, (b) and (e) $C_{10}E_3P_3S$, and (c) and (f) $C_{10}P_3E_3S$.

Table 3 Diffusion coefficients of $C_{10}E_3P_3S$, $C_{10}P_3E_3S$ and $C_{10}E_3S$

Sample	Concentration (g L^{-1})	$D_{t\to0}$ (m^2 s^{-1})	$D_{t\to\infty}$ (m^2 s^{-1})	$D_{t\to\infty}/D_{t\to0}$
$C_{10}E_3P_3S$	1.0	4.03×10^{-11}	1.40×10^{-13}	3.49×10^{-3}
	1.0×10^{-1}	4.68×10^{-10}	8.67×10^{-12}	1.85×10^{-2}
	1.0×10^{-2}	1.64×10^{-8}	2.49×10^{-10}	1.52×10^{-2}
	1.0×10^{-3}	4.50×10^{-6}	2.26×10^{-8}	5.02×10^{-3}
$C_{10}P_3E_3S$	1.0	4.57×10^{-11}	7.22×10^{-15}	1.58×10^{-4}
	1.0×10^{-1}	5.97×10^{-10}	1.02×10^{-12}	1.72×10^{-3}
	1.0×10^{-2}	4.13×10^{-8}	2.88×10^{-11}	6.97×10^{-4}
	1.0×10^{-3}	4.38×10^{-6}	4.05×10^{-8}	9.26×10^{-3}
$C_{10}E_3S$	1.0	1.56×10^{-11}	2.29×10^{-14}	1.98×10^{-3}
	1.0×10^{-1}	1.42×10^{-10}	1.38×10^{-12}	9.73×10^{-3}
	1.0×10^{-2}	1.81×10^{-8}	5.95×10^{-11}	3.28×10^{-3}
	1.0×10^{-3}	1.25×10^{-6}	2.75×10^{-8}	2.19×10^{-2}

$\gamma_{(t)t\to0}$ and $\gamma_{(t)t\to\infty}$ are linearly related to $t_{1/2}$ and $t_{-1/2}$, respectively, and their curves are shown in Fig. 6. The slopes of the curves can be obtained after fitting to obtain the diffusion coefficients $D_{t\to0}$ and $D_{t\to\infty}$, and the related results are shown in Table 3.

If the surfactant molecules are only controlled by diffusion during adsorption, then eqn (12) and (13) should be linear curves; however, the curves in Fig. 6 show that there are inflection points in both the $t_{1/2}$ and $t_{-1/2}$ *versus* surface tension curves, which leads to the inference that adsorption of $C_{10}E_3S$, $C_{10}E_3P_3S$, and $C_{10}P_3E_3S$ is not only controlled by diffusion.

As can be seen from Table 3, for the same sample, $D_{t\to\infty}$ is always smaller than $D_{t\to0}$ at the same concentration, which may

be due to the fact that in the early stage of adsorption, the intermolecular force and adsorption barrier are relatively small; in the late stage of adsorption, the surfactant molecules aggregated on the surface of the gas–liquid interphase may diffuse to the bulk phase in the opposite direction, and the diffusion rate of the molecules that are not adsorbed slows down. The diffusion coefficients of the $C_{10}E_3P_3S$ and $C_{10}P_3E_3S$ are one order of magnitude larger than those of the $C_{10}E_3S$. The diffusion coefficients of $C_{10}E_3P_3S$ and $C_{10}P_3E_3S$ are one order of magnitude larger than those of $C_{10}E_3S$. This may be due to the fact that $C_{10}E_3P_3S$ and $C_{10}P_3E_3S$ have higher charge densities which contribute to their aggregation towards the surface at the early stage of adsorption, and the presence of sulfate bonds in
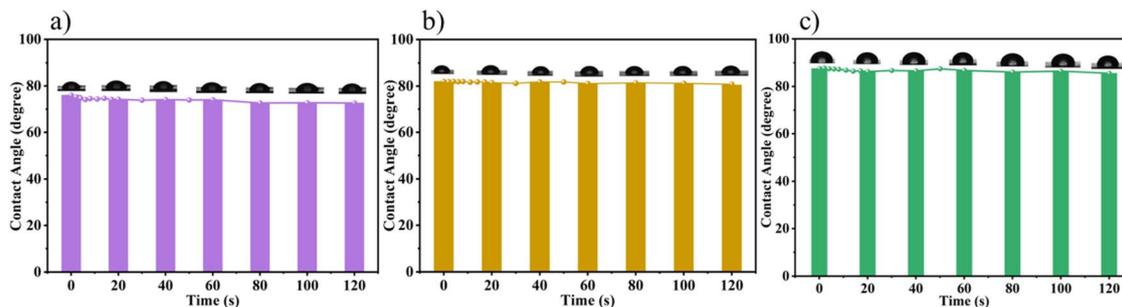
Fig. 7 Dynamic contact angle of (a) $C_{10}P_3E_3S$, (b) $C_{10}E_3P_3S$ and (c) $C_{10}E_3S$ on a paraffin film at a concentration of 1 g L^{-1}.

the molecules makes it easier to form hydrogen bonding interactions with the molecules of the adsorbed layer, so that the influence of the adsorption potential on the late stage of the adsorption of $C_{10}E_3S$ is smaller than that of $C_{10}E_3P_3S$ and $C_{10}P_3E_3S$. Additionally, $D_{t\to\infty}/D_{t\to0}$ is less than 1, which indicates that the adsorption process belongs to mixed diffusion-kinetics adsorption mechanism.[40]

3.5 Contact angle measurement

The contact angle, denoted as θ, is defined as the angle measured from the solid–liquid interface, passing through the interior of the liquid, to the gas–liquid interface at the triple-phase junction of the solid, liquid and gas phases. The relationship between the equilibrium contact angle and the three interfacial free energies is typically described by the Young's equation:[41]

$$\gamma_{gs} = \gamma_{ls} + \gamma_{gl}\cos\theta \tag{14}$$

In eqn (14), θ is the equilibrium contact angle of the surfactant droplet on the paraffin matrix membrane. γ_{gs}, γ_{gl} and γ_{ls} are the solid–gas interfacial tension, liquid–gas interfacial tension and solid–liquid interfacial tension, respectively. Under the condition that the liquid medium is water and the solid medium is paraffin film, γ_{gs} and γ_{gl} can be considered as constants. Therefore, the contact angle θ will change with the change in interfacial tension.

From Fig. 7, it can be seen that with the increase in time, the contact angle gradually decreases but the change is not obvious, which indicates that the solid–liquid interface can remain stable and the surface adsorption is less. The size of contact angle is as follows: $C_{10}E_3S > C_{10}E_3P_3S > C_{10}P_3E_3S$, which indicates that the molecules containing only EO groups are more hydrophilic and not easy to be adsorbed on the paraffin film. Introducing PO group into the molecule can change the polarity of the molecule and thus make it easy to be adsorbed on the paraffin film. At the same time, when PO precedes EO, it increases the branching effect of the molecule and makes it easier to be adsorbed on paraffin film.

3.6 Emulsifying power

One of the most important functions of surfactants is to facilitate the formation of stable emulsions in certain systems.[42]
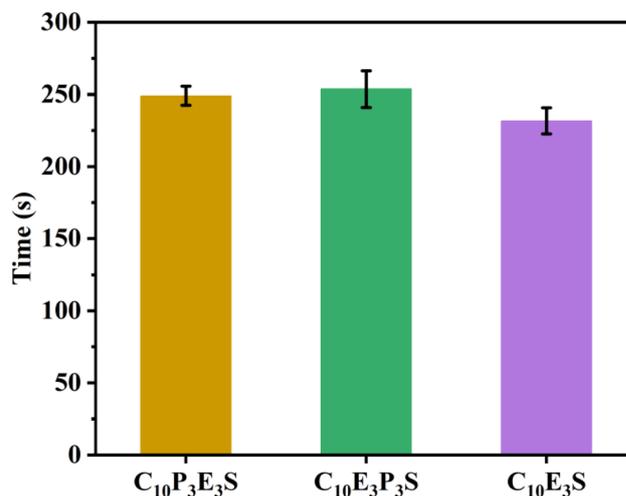

Fig. 8 Emulsifying power of $C_{10}P_3E_3S$, $C_{10}E_3P_3S$ and $C_{10}E_3S$.

Using paraffin liquid as the oil phase while surfactant solution as the aqueous phase, their emulsification properties were investigated, and the results are shown in Fig. 8.

As the number of PO groups in the molecule increases, the phase separation time of the emulsified system increases, which is attributed to the lipophilicity of the PO groups. The introduction of PO groups into the molecule enhances the interaction forces between the surfactant molecules and the oil phase molecules, which results in a longer phase separation time.

3.7 Wettability

When the canvas sheet is submerged in a certain concentration of surfactant solution, the solution gradually replaces the air in the voids of the canvas sheet.[43] The shorter the canvas drop, the better the surfactant penetration.

In the textile industry, surfactants are commonly used in an alkaline environment,[44] and products with a certain level of alkali resistance have a higher working efficiency in this environment. The wettability of $C_{10}E_3S$, $C_{10}P_3E_3S$ and $C_{10}E_3P_3S$ at different alkali concentrations is shown in Fig. 9.

From Fig. 9, it can be seen that $C_{10}P_3E_3S$ has the best alkali wettability resistance, which may be attributed to its low γ_{cmc}, and the low surface tension of the solution makes it easier for the hydrophobic groups in the surfactant molecules to adsorb
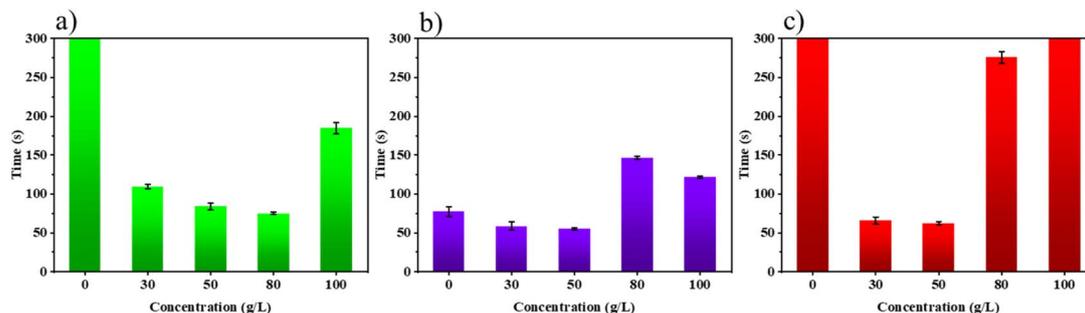
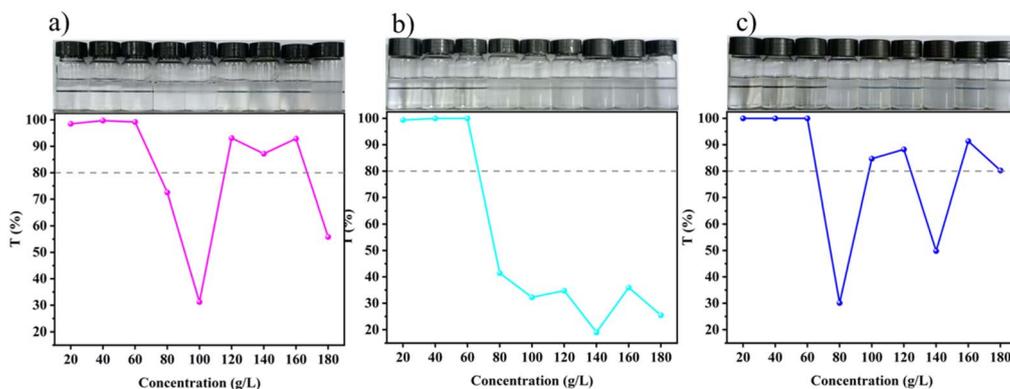Fig. 9   Wettability of (a) $C_{10}E_3S$, (b) $C_{10}P_3E_3S$ and (c) $C_{10}E_3P_3S$.

Fig. 10   Light transmittance diagrams and appearance under different NaOH concentrations of (a) $C_{10}E_3S$ (b) $C_{10}E_3P_3S$ and (c) $C_{10}P_3E_3S$.

on the surface of the canvas while the hydrophilic headgroups are in the solution. This shows consistency with the results of the contact angle tests. The permeability of $C_{10}E_3S$ and $C_{10}E_3P_3S$ was poorer when the NaOH solution was absent, which could be attributed to the larger γ_{cmc}, the incomplete formation of micelles by surfactant molecules in solution, and the low ability to reduce the surface tension, which led to a longer settling time of the canvas sheets.

3.8   Alkali tolerance

In the alkaline boiling and oxygen bleaching process of cotton fabrics, surfactants are usually used as refining agents to maintain the penetration and synergistic decontamination functions in a strong alkaline environment, and their alkali resistance directly determines the application efficiency. Fig. 10 shows the alkali resistance data of (a) $C_{10}E_3S$, (b) $C_{10}E_3P_3S$ and (c) $C_{10}P_3E_3S$.

As is evident from Fig. 10, $C_{10}E_3P_3S$ and $C_{10}P_3E_3S$ have poorer alkali resistance at higher alkali concentrations and better alkali resistance at lower alkali concentrations. In comparison, the alkali resistance of $C_{10}E_3S$ is generally stronger than that of the other two, and its alkali resistance can reach 160 g L^{-1}. The low ionic strength of OH^- may disrupt the hydration layer surrounding micelles, leading to reducing micelle stability. As the ionic strength continues increasing, the
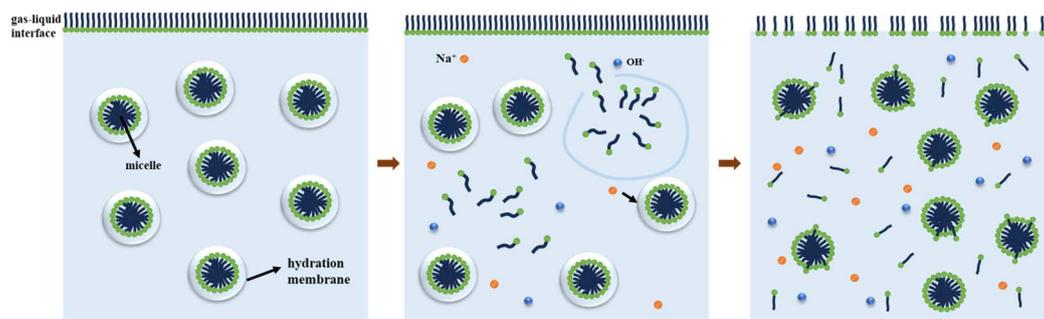
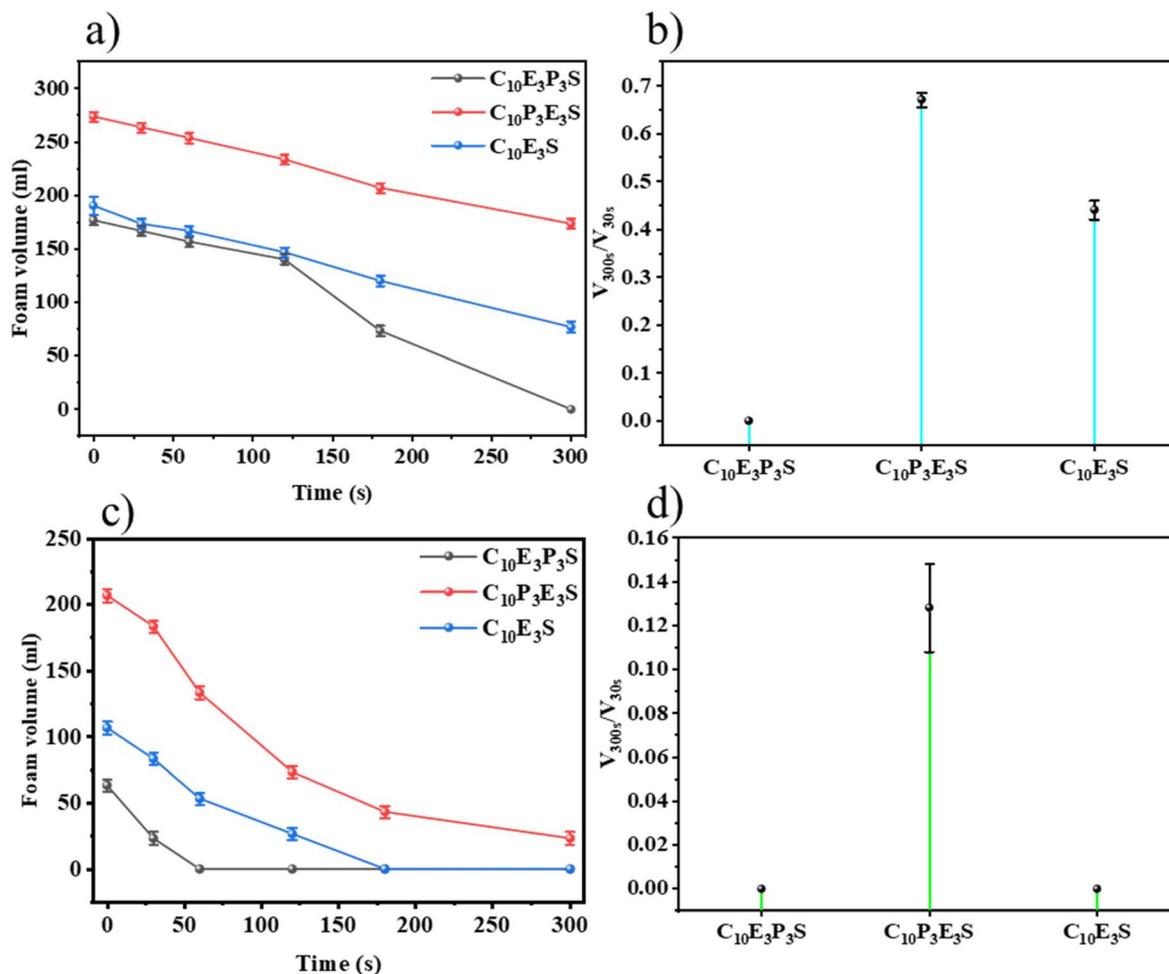Scheme 1   Micelle change process upon addition of NaOH to a surfactant solution.

Fig. 11 Foaming ability at (a) 25 °C and (c) 50 °C and foam stability of different surfactant solutions at (b) 25 °C and (d) 50 °C.
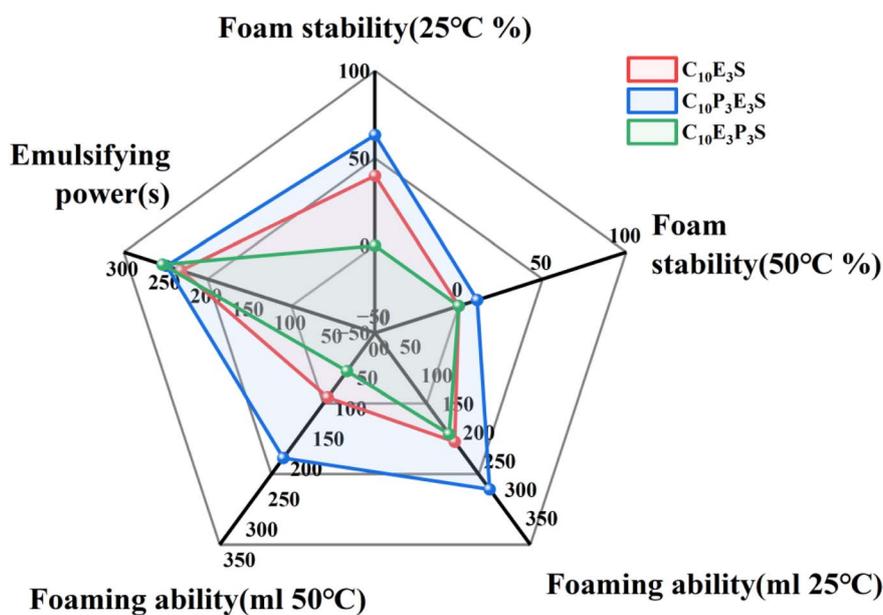

Fig. 12 Application properties of $C_{10}E_3S$, $C_{10}E_3P_3S$ and $C_{10}P_3E_3S$.

hydration layers surrounding numerous micelles are disrupted, the diffusion double layer of ionic groups are compressed,[45] the electrostatic repulsion between charges is shielded, and the compact molecular arrangement also increases the micelle aggregation number. Meanwhile, the excessive Na^+ may compete with polyethylene oxide chains to bind water molecules, thus weakening the hydration of polyethylene oxide chains. In this period, the micelle aggregation number is relatively large, but the number of micelles is relatively small, causing the solution to appear turbid (Scheme 1). As can also be seen from Fig. 10, the apparent state of the solution does not become more turbid with the increasing concentration of NaOH, and the mechanism behind this phenomenon warrants further investigation.

3.9 Foam ability and foam stability

The foam properties of the surfactants were tested using the modified Ross–Miles method, and the results are shown in Fig. 11.

When the test temperature was increased from 25 °C to 50 °C, the foaming ability and foam stability of the three surfactant solutions decreased, which may be attributed to the fact that the rupture process of the foam liquid film, which is not a thermodynamically stable system, was accelerated by the external energy input. In addition, by comparing Fig. 7 with 9, it can be found that there is a relationship between foaming ability and wettability. This suggests that $C_{10}E_3P_3S$ has potential for application in textile printing and dyeing. Comparing the molecular structures of $C_{10}E_3S$, $C_{10}P_3E_3S$ and $C_{10}E_3P_3S$, it is not difficult to find that the steric hindrance of $C_{10}P_3E_3S$ may be increased due to the forward position of the PO group, which further enhances the strength and elasticity of the liquid film.

4   Conclusion

In this research, three branched alcohol ether sulfates, namely $C_{10}E_3S$, $C_{10}E_3P_3S$ and $C_{10}P_3E_3S$, were successfully synthesized within a sulphuric sulphonation unit. Their structures were characterized using FT-IR spectroscopy, TGA and ESI-MS. Subsequently, a comprehensive investigation was conducted on their dynamic surface tension, static surface tension, contact angle, and wettability. Due to its distinctive molecular structure, $C_{10}P_3E_3S$ exhibited outstanding performance in reducing surface tension, thereby enhancing wettability, which suggests its potential application in the textile industry (Fig. 12). Moreover, it demonstrated superior emulsification properties. In contrast to $C_{10}P_3E_3S$, the incorporation of PO groups into EO groups in $C_{10}E_3P_3S$ led to inferior foam properties. This characteristic expands the potential applications of $C_{10}E_3P_3S$ in low-foaming scenarios, such as industrial cleaning. Furthermore, the surfactants we have tested may have the ability in enhanced oil recovery and applications in softness, which can be further studied. Besides, the mixture system properties of $C_{10}E_3S$, $C_{10}E_3P_3S$ and $C_{10}P_3E_3S$ with other surfactants such as APG (alkyl polyglucoside), AEO (fatty alcohol-polyoxyethylene ether) and

AEB (butoxylated alkyl *block* ether) can be further researched. In addition, some mechanistic insights in this study such as alkali tolerance, wettability and foaming ability require deeper discussion.

Conflicts of interest

The authors declare that they have no known competing financial interests or personal relationships that could have appeared to influence the work reported in this paper.

Data availability

The data used in this study come from publicly accessible databases and data generated through experiments. Public datasets can be accessed through major databases. However, due to ethical and privacy restrictions, some experimentally generated data are not suitable for direct public release. To ensure the reproducibility of the study and the transparency of the results, we are willing to provide the necessary data support upon reasonable request.

Supplementary information is available. See DOI: **https://doi.org/10.1039/d5ra05419b**.

References

1 G. Zhao, B. Zhu, Z. Dou, P. Yan and J. Xiao, *Colloids Surf., A*, 2008, **327**, 122–126.

2 U. Baù, F. Mangani, A. Roccon and A. Soldati, *Langmuir*, 2025, **41**, 18488–18500.

3 R. Kashapov, A. Lykova, N. Kashapova, A. Ziganshina, T. Sergeeva, A. Sapunova, A. Voloshina and L. Zakharova, *Food Hydrocolloids*, 2021, **113**, 106449.

4 M. Sarafidou, A. C. Mendes, D. Ladakis, T. Tsironi and A. Koutinas, *Food Hydrocolloids*, 2025, **168**, 111531.

5 Y. Yang, J. Hao and J. Cui, *Curr. Opin. Colloid Interface Sci.*, 2024, **72**, 101819.

6 J. Yang, *J. Colloid Interface Sci.*, 2004, **274**, 237–243.

7 B. Pérez-Cid, X. Vecino, A. López-Prieto, C. Serra-Rodríguez, J. M. Cruz and A. B. Moldes, *Chem. Biol. Technol. Agric.*, 2025, **12**, 72.

8 C. Vakh and S. Koronkiewicz, *TrAC, Trends Anal. Chem.*, 2023, **165**, 117143.

9 Q. Dong, X. Li and J. Dong, *Colloids Surf., A*, 2022, **649**, 129419.

10 S. Yada, Y. Yoshioka, M. Ohno, T. Koda and T. Yoshimura, *Colloids Surf., A*, 2022, **648**, 129247.

11 Z. Jin, Z. Xu, Q. Gong, S. Zhao and J. Yu, *J. Dispersion Sci. Technol.*, 2011, **32**, 898–902.

12 Q. Zhang, Y. Li, Y. Song, J. Li and Z. Wang, *Colloids Surf., A*, 2018, **538**, 361–370.

13 J. Chen, X. Hu, Y. Fang and Y. Xia, *J. Mol. Liq.*, 2020, **311**, 113276.

14 C. Xu, T. Zhang, S. Wang, J. Gan and H. Wang, *Processes*, 2025, **13**, 1612.

15 S. M. S. Hussain, M. S. Kamal, L. T. Fogang and S. Patil, *J. Mol. Struct.*, 2019, **1196**, 851–860.

16 J. Zeng, J. Ge, G. Zhang, H. Liu, D. Wang and N. Zhao, *J. Dispersion Sci. Technol.*, 2010, **31**, 307–313.

17 X. Liu, Y. Zhao, Q. Li and J. Niu, *Colloids Surf., A*, 2016, **494**, 201–208.

18 A. Klaus, G. J. T. Tiddy, D. Touraud, A. Schramm, G. Stühler and W. Kunz, *Langmuir*, 2010, **26**, 16871–16883.

19 M. N. Khan, W. R. Wan Sulaiman and A. H. Abbas, *Arabian J. Sci. Eng.*, 2021, **46**, 6915–6924.

20 Z. Chen, X. Lin, Q. Chen, B. Song, X. Pei and Z. Cui, *J. Surfactants Deterg.*, 2024, **27**, 937–948.

21 X. Huang, L. Sun, S. Cao, W. Xie, Y. Huo, X. Liu and J. Xia, *J. Mol. Liq.*, 2024, **408**, 125135.

22 M. J. Marand, M. Pero, M. Ahmadi, K. Nayebzadeh, M. Farhoodi, L. Mirmoghtadaie and S. M. Hosseini, *Carbohydr. Polym.*, 2025, **356**, 123228.

23 M. A. Abd El-Ghaffar and M. S. Hashem, *Carbohydr. Polym.*, 2013, **92**, 2095–2102.

24 A. S. Montaser and F. A. Mahmoud, *Int. J. Biol. Macromol.*, 2019, **124**, 659–666.

25 Y. Zhang, W. Bei and Z. Qin, *Materials*, 2020, **13**, 865.

26 N. Pal, N. Saxena, K. V. Divya Laxmi and A. Mandal, *Chem. Eng. Sci.*, 2018, **187**, 200–212.

27 J. Hao, T. Qin, Y. Zhang, Y. Li and Y. Zhang, *Colloids Surf., B*, 2019, **181**, 814–821.

28 T. Zhao, N. Feng, Y. Zhao and G. Zhang, *Colloids Surf., A*, 2020, **606**, 125482.

29 S. Hou, Y. Wang, J. Li, Z. Wang, Y. Jiang and T. Geng, *Colloids Surf., A*, 2023, **656**, 130523.

30 R. Kamboj, S. Singh and V. Chauhan, *Colloids Surf., A*, 2014, **441**, 233–241.

31 C. Gong, T. Zhao, Y. Zhao and G. Zhang, *J. Mol. Liq.*, 2022, **345**, 117044.

32 G. Wang, W. Qu, Z. Du, Q. Cao and Q. Li, *J. Phys. Chem. B*, 2011, **115**, 3811–3818.

33 W. Yang, Y. Cao, H. Ju, Y. Wang, Y. Jiang and T. Geng, *J. Mol. Liq.*, 2021, **326**, 115339.

34 M. Guo, J. Li, X. Yi, L. Qiu, L. Zhou, X. Li, L. Liu and J. Dong, *Colloids Surf., A*, 2025, **723**, 137379.

35 M. J. Rosen and L. D. Song, *J. Colloid Interface Sci.*, 1996, **179**, 261–268.

36 X. Zhang, S. Cao, C. Gao, Y. Huo, X. Huang and X. Liu, *J. Dispersion Sci. Technol.*, 2025.

37 Q. Zhang, Y. Li, Y. Song, H. Fu, J. Li and Z. Wang, *J. Mol. Liq.*, 2017, **243**, 431–438.

38 V. B. Fainerman, A. V. Makievski and R. Miller, *Colloids Surf., A*, 1994, **87**, 61–75.

39 K. J. Mysels, *J. Phys. Chem.*, 1982, **86**, 4648–4651.

40 L. Zhi, Q. Li, Y. Li and Y. Song, *Colloid Polym. Sci.*, 2014, **292**, 1041–1050.

41 F. Gonzalez-Caballero and M. L. Kerkeb, *Langmuir*, 1994, **10**, 1268–1273.

42 S. Li, B. Jiao, S. Faisal, Y. Zhang, B. Wu, W. Li, A. Shi, H. Liu and Q. Wang, *Food Hydrocolloids*, 2023, **134**, 108078.

43 S. Liu and A. Ben-Abdelwahed, *Colloids Surf., A*, 2025, **720**, 136991.

44 Z. Bi, Y. Wu, G. Chen, X. Li and J. Dong, *Chem. Eng. J.*, 2024, **499**, 156395.

45 G. Deng, S. Yao and D. Lin, *World J. Microbiol. Biotechnol.*, 2005, **21**, 1209–1214.